

Mesoporous Thin Films for Fluid Manipulation

Magalí Mercuri, Claudio L. A. Berli,* and Martín G. Bellino*

The ability to control nanoflows is critical to design and fabricate ever more versatile nanosystems. Scientists are currently interested in finding ways to handle fluid dynamics inside nanoporous networks, not only to increase our knowledge of fluidic behavior but also to develop novel nanodevices that have potential utility in applications ranging from diagnostics to the production of high-value chemicals. Here, we demonstrate how fluid motion can be manipulated by controlling the coexisting infiltration and evaporation phenomena in mesoporous films. A versatile actuation approach through liquid–vapor dynamic modulation was developed by integrating mesoporous substrates with a thermoelectric cell. This actuation resulted in fast and reversible fluid displacements through the mesoporous matrix, which was achieved with relatively small temperature variations by controlled voltage inputs. The versatility of the strategy is demonstrated by tunable cycling of fluid imbibition and switched nanofluidic connection of liquids into the substrate. This novel nanoflow manipulator could be the basis for smart nanofluidic devices toward exciting applications in actuators, controlled pattern formations and release systems.

Active control of nanoflows presents substantial challenges in both scientific and engineering aspects.^[1,2] Although applications of mesoporous thin films in technologies such as biocatalysis,^[3] electrochemistry,^[4] and optical sensing^[5,6] have been reported, the emergent properties of these nanostructures to actuate fluid transport have not been explored yet. This work demonstrates how fluid motion can be manipulated by controlling the coexisting infiltration and evaporation phenomena in mesoporous substrates (2–50 nm pore size according to International Union of Pure and Applied Chemistry (IUPAC) definition^[7]). A flexible actuation strategy was designed by integrating mesoporous thin films with a thermoelectric cell. The liquid–vapor interface was set in motion by changing substrate temperature, which is carried out by controlled voltage inputs. This joystick-like actuation resulted in fast and reversible displacements of the fluid through the mesoporous film, which


was achieved with relatively small temperature variations. Besides, handling the fluid front from different reservoirs enables a switched nanofluidic connection of liquids into the substrate. This dynamic control over the movement of fluids at the micrometer scales is a first step toward exciting applications in actuators, micro/nanodevices, and functional coatings.

The confined spaces of mesoporous oxide thin films (MOTF) are open both to large-area integration with matter and the miniaturization of materials and functional devices.^[8,9] An additional relevant advantage of MOTF is the possibility to infiltrate fluids through the porous structure by exploiting capillary action. When sessile drops are deposited on mesoporous films, capillary infiltration quickly forms an annular region of wetted material.^[10,11] Annuli have a steady width, which results from the balance between capillary infiltration and liquid evaporation,

as described by a simple transport model.^[10] Thus, for a given temperature, the advancement of liquid–vapor interface into the porous matrix is arrested at a defined position. Taking into account the temperature dependence of model parameters (evaporation rate, fluid density, viscosity, and surface tension)^[10] one may readily predict the annulus width variation with temperature. On the base of these calculations, we designed a strategy to manipulate fluid transport, and experimentally prove it, as described next. In fact, we developed a novel electrically actuated nanofluidic-transport system, which can easily trigger the displacement of liquid–vapor interface in a targeted area of MOTF by imposing a locally controlled temperature field. Our designed approach is based on the dynamics of liquid–vapor interface in nanosystems^[12,13] and provides a starting point for the exploration of smart fluid delivery systems as a versatile tool for a new scenario in nanomaterial applications, for instance in switched nanochemistry devices. An additional advantage is the “open-pit” nanofluidic nature of the strategy,^[14] which obviates the usually costly steps of sealing and tubing in the fabrication of microdevices. It is worth noting that works dealing with the manipulation of small flows on mesoporous materials are just starting to emerge in the literature. Notable examples are actuation of the capillary imbibition through the electrical control of the solid–liquid interfacial tension in nanoporous gold^[15] and the light-induced manipulation of droplets on nanostructured titania surfaces.^[16] In advantage to these methods, our technique does not require electrolyte solutions or surface pretreatment with photoresponsive additives because fluid handling is achieved by altering the natural phenomenon of surface

M. Mercuri, Dr. M. G. Bellino
 Comisión Nacional de Energía Atómica
 Av. Gral. Paz 1499, San Martín B1650KNA, Argentina
 E-mail: mbellino@cnea.gov.ar

Dr. C. L. A. Berli
 INTEC (Universidad Nacional del Litoral-CONICET)
 Predio CCT CONICET Santa Fe
 RN 168, 3000 Santa Fe, Argentina
 E-mail: cberli@santafe-conicet.gov.ar

 The ORCID identification number(s) for the author(s) of this article can be found under <https://doi.org/10.1002/admi.201700970>.

DOI: 10.1002/admi.201700970

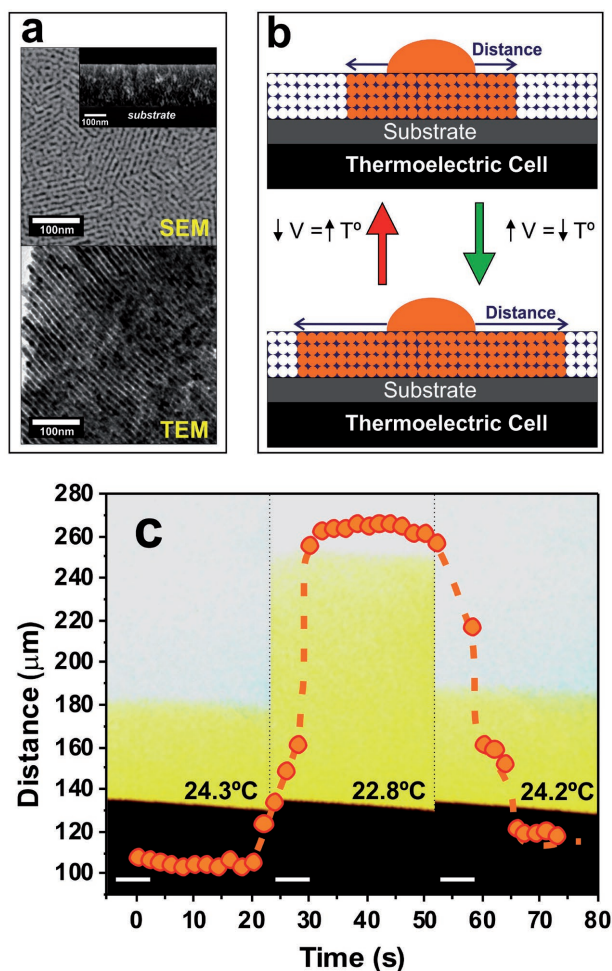


Figure 1. Thermoelectrical control of fluid movement. a) Scanning electron microscope (SEM) and transmission electron microscope (TEM) images of aligned pores domains in the MOTF, showing the typical conduit-like mesostructure. The inset in the SEM image shows a profile cut. b) Schematic illustration of the experimental setup and procedures for manipulating fluids into mesoporous films by controlling substrate temperature with a thermoelectric cell. c) Displacement of the fluid front from its initial position as a function of time. Voltage varied from 0 to 2 V and return to 0 V in steps of 0.07 V s^{-1} . The direction of motion is the same as the voltage direction. The dotted line is only a guide to the eye. Inset: Optical images where the fluid is moving along the mesoporous film by thermoelectric actuation. The left-right and medium images represent the fluid front at 0 and 2 V, respectively. Sample temperature for steady states and greatest increase of wetted region are shown in the respective inserted images. Scale bars = $50 \mu\text{m}$.

evaporation. For this purpose here we control the mesoporous film temperature by means of a Peltier cell; nevertheless one might also employ an infrared laser to locally change the surface temperature, thus expanding the versatility of the proposal.

The combination of sol-gel synthesis^[17] and template self-assembly was used to build uniform titania films with highly porous structure (Figure 1a) on a silicon wafer.^[9,10] Films were 180 nm thick, 50% porous and presented pore and neck sizes of 6 and 4.1 nm, respectively, as measured by environmental ellipsometric porosimetry (EEP, Figure S1, Supporting Information). In ambient conditions, the silicon substrate was

brought in contact with a thermoelectrical device (Peltier cell, see Figure 1b), which creates a temperature difference when a voltage is applied.^[18] This allows us to tune the temperature field applied directly to the mesoporous film. In this way, the balance between capillary filling from the liquid drop and mass loss due to evaporation to the environment can be shifted to different levels, and the overall result is that the liquid-vapor interface position can be electrically actuated. The ability to use voltage control for motion of fluid-front in an MOTF is illustrated in Figure 1c. Starting from a steady annulus at $24.3 \text{ }^\circ\text{C}$, the fluid-front gradually moves straight ahead after a linear voltage change is applied (0–2 V—cooling from 24.3 to $22.8 \text{ }^\circ\text{C}$), as illustrated by optical microscopy (Figure 1c and Movie S1, Supporting Information). This decrease in the local temperature (from the room temperature value in our laboratory) weakens the liquid evaporation rate, and capillary filling drives an advancement of the fluid front. It is worth to remember here that evaporation rate is proportional to the wetted surface, while the infiltration rate is inversely proportional to the fluid-front distance.^[10] Thus, after a temperature variation, a new balance is established at a different fluid-front position. The wetted region can be clearly seen because it produces a refractive index contrast in relation to the dry zone (see Figure S1, Supporting Information, and also refs. ^[10] and ^[14] for discussions on fluid-front roughening).

For a given temperature and relative humidity (RH), the annulus reaches a steady state width as capillary infiltration and evaporation counterbalance.^[10] The evaporation rate (mass loss per unit surface area) can be expressed as $m_{ev} = D_v(d\rho/dz)_s$, where D_v is the vapor diffusion coefficient, ρ is the vapor density, and z is the coordinate normal to the film-air interface. By using Dalton law, the above expression can be rewritten in terms of the vapor pressure: $m_{ev} \sim (dp/dz)_s$. The air in direct contact with the film surface is saturated in vapor, p is the saturated vapor pressure p_{sat} , which strongly depends on temperature. Assuming that the diffusive vapor transport takes place through a boundary layer of thickness δ , where the $p(z)$ decreases from p_{sat} to the ambient vapor pressure $p_a = RHp_{sat}$, the evaporation rate results $m_{ev} \sim p_{sat}(1 - RH)/\delta$.

In normal conditions, evaporation causes a heat flux from the evaporative surface toward the environment, which produces a rapid cooling. The surface temperature (T_s) decreases, so does the evaporation rate, and when T_s reaches the wet-bulb temperature, the system equilibrates (all the heat is consumed to evaporate water). When the Peltier cell is activated, heat extraction suddenly diminishes temperature T_s , hence p_{sat} , and consequently m_{ev} . This effect produces an imbalance between water loss and infiltration rate, and the fluid front advances up to a new steady state position, as it is clearly seen in the experiments. It should be noted however that the growing of the annulus width observed in practice is larger than the one predicted for the variations of $m_{ev}(T)$ alone, according to the model reported in ref. [10]. We later discuss the nature of the unexpectedly large displacement of the fluid front.

Furthermore, to realize the reversible regulation of nanoflow, we investigated the switchback control of the movements in the mesoporous network. The direction of the fluid-front's movement is easily controlled using this voltage switchback feature (2–0 V—heating from 22.8 to $24.2 \text{ }^\circ\text{C}$) in a similar manner to

that of an electric train (Figure 1c and Movie S1, Supporting Information). In other words, increase in voltage led to a lower temperature, and then a diminution of the liquid evaporation. As a result, the wetted zone incremented from their original position. Upon voltage decreasing, temperature increased, hence the fluid evaporation, and the fluid-front returned to their original state. Therefore, by electrically adjusting the temperature level using the Peltier cell (and thus regulating the degree of evaporation rate), we can control the fluid-front position of the infiltration at will by small temperature variations. Occasionally, the fluid moves in a stepwise fashion, such as the translational motion shown in Movie S1 in the Supporting Information. Such stepwise motion suggests that the fluid must eventually overcome a series of periodic barriers. This effect is surely related to the oscillating behavior that eventually presents the fluid front in these systems, as recently reported.^[10] In addition, the effective motion that we obtain from our voltage/temperature-responsive method contains an inertial contribution from the response time of this coupled system. Even if the procedure has not been yet fully optimized, and several technical improvements can be made, the above results indicate that thermally driven nanoflow can be electrically actuated in an MOTF.

We additionally examined the ability of the presented strategy to withstand several cycles of forward and backward movements. In Figure 2, we present the response to a cycled voltage input, which demonstrates the capability of the infiltration zone to change between stationary and activated states while maintaining their nanofluidic integrity. As can be seen in the figure, this fluid motion sequence is repeatable over five cycles. The possibility to perform additional cycles is only limited by the drop evaporation. The thermal actuator exhibited fluid-wave translation from an alternating triangular waveform voltage input. Movie S2 in the Supporting Information depicts the cycling process accelerated by a factor about 5. This cycling sequence is according to voltage input described in the caption of Figure 2.

We further capitalized on this new active actuation of the fluid by expanding their capabilities to switch the fluidic connection between a pair of droplet. Wetted areas nucleate from the two droplet-landmarks and grow via increase voltage (0–1 V). Liquids are transported through the mesoporous network up to the point in which the annulus borders meet, forming a connection between fluids, as shown in Figure 3. Movie S3 in the Supporting Information depicts the switched process accelerated by a factor 5. When the potential was inverted (1–0 V), the annulus borders moved back, in other words, the connection was switched off (see Figure 3 and Movie S3, Supporting Information). Note that profiles of color intensity across droplets (Figure 3a) provide a visual analogy for determining the switched communication into the mesoporous films. Figure 3b remarks how on/off connections formed between isolated pairs of droplet-seeds. This controlled on/off communication approach could be a route to the development of nanofluidic logic circuits and time-regulated chemical reactions on mesoporous films.

In summary, here we communicate the development of a novel method to manipulate nanoflow: a thermally driven transport into mesoporous films that is actuated by the

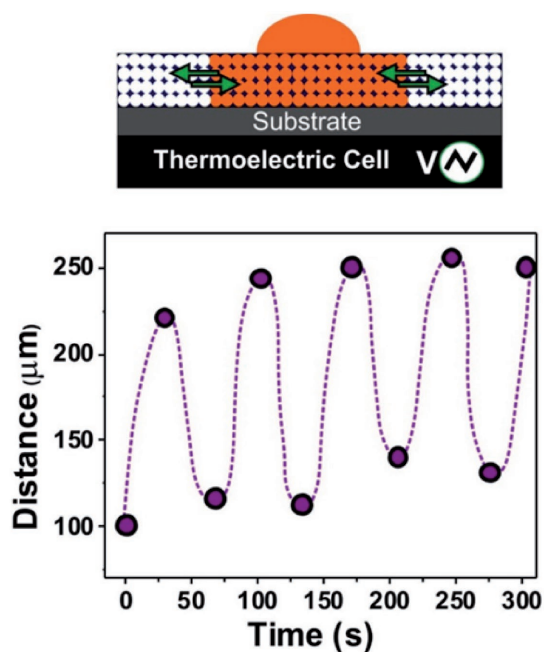


Figure 2. Cycling of the fluid motion into the mesoporous network. Distance in response to a triangular voltage input. Five cycles of forward and backward displacements were realized. Cycles were initiated in the steady state and for each active change 0–2 V (0.015 Hz) were applied. The schematization of the cycled actuation process is shown above the graphic. The dashed line is a guide to the eye.

application of voltage. The mesoporous film temperature can be locally controlled and, thereby, the infiltration–evaporation competition can be tuned. This allows one to accurately handle liquid infiltration as it were produced by a clever capillary pump.

The unexpectedly large displacement of the fluid front may be understood by taking into consideration the condensation phenomenon. The wet annulus creates a microclimate of increased vapor concentration over the film surface, as well as in the close vicinity ahead of the fluid front. It is worth to remember here that mesoporous films are very effective in capturing vapor, as nanopores strongly decrease the vapor pressure p required for condensation, in relation to a uniform solid surface. According to Kelvin equation, condensation will proceed if $p > p_{\text{sat}} \exp(-p_c V_m / RT)$, where R is the gas constant, V_m is molar volume of the liquid, and p_c is the capillary pressure, which is inversely proportional to the pore size. It is readily seen that decreasing temperature T favors vapor condensation near the fluid front, as the right-hand side of the above inequality decreases. Therefore, decreasing temperature by means of the Peltier cell produces a displacement of the fluid front by a twofold effect: a uniform decrease of evaporation rate and an increase of condensation in the close vicinity of the annulus border, where a saturated microclimate zone develops. Evaporation rate is the controlling mechanism for the annulus width, but the induction of vapor condensation ahead of the fluid front would be inherently associated.

This methodology is fully compatible with the techniques and substrates used in the sensor, microfluidic, and microelectronics industry, opening a path to manipulate ultrasmall

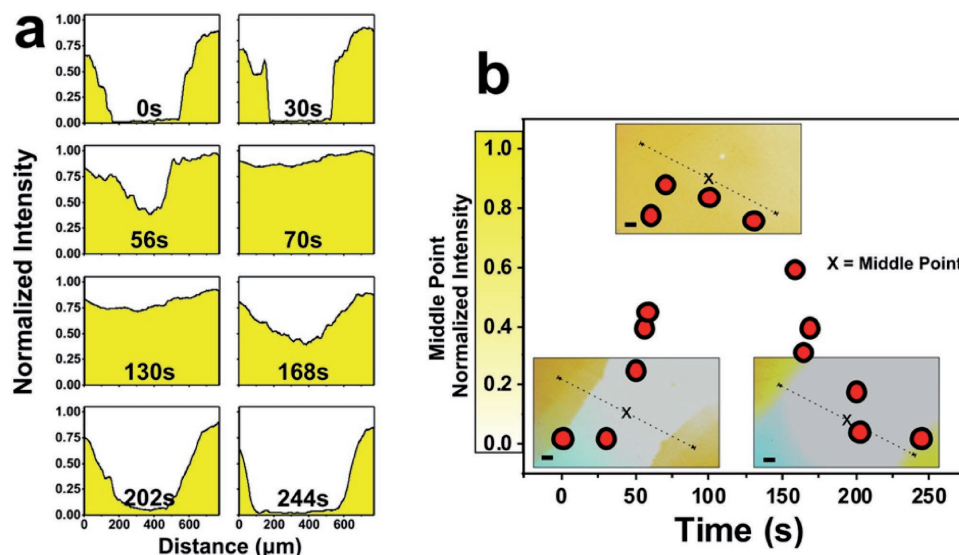


Figure 3. Switched nanofluidic connection between droplet-landmarks. a) Time-lapse sequence of line profiles of color intensity across two droplets (interdroplet distance = 1 mm) showing the initial stage, the nanofluidic connection between the annuli, and the switched off connection. White color corresponds to the dry film and yellow color corresponds to a wetted region. b) Normalized color intensity versus time for the middle interdroplet point. Nanofluidic connection occurs when the middle point between drops turns yellow. Inset pictures are optical microscopy images illustrating the switched on/off connection at the respective times. The dashed lines and X points correspond to the places where color profiles a) and middle point intensity b) were measured, respectively. Scale bars = 50 μm.

amounts of liquid in novel nanodevices. Alternative voltage/temperature conversion strategies according to the need may be used for an additional improvement in the versatility of the method.^[19,20] Therefore, it may be concluded that the designed principle as well as the demonstrated nanoflow manipulator, could be the basis for new functional coating and smart nanofluidic devices intended for a variety of applications, including actuators, controlled pattern formation, and release systems. More complex applications might include confining genetic material and performing biochemical reactions or parallel drug or toxin screening. Furthermore, precise and localized heaters can be readily integrated to microfluidic platforms nowadays,^[21] which ensures the potential implementation of the proposed technology.

Experimental Section

Film Synthesis and Characterization: Mesoporous thin films were produced by evaporation-induced self-assembly.^[8,9] For this purpose, 25 × 25 mm² silicon substrates were dip coated at 20% RH and 3 mm s⁻¹ withdrawal rate. TiCl₄ was used as the inorganic precursor, and Pluronic F127 ((EO)₁₀₆(PO)₇₀(EO)₁₀₆, where EO and PO represent ethylene oxide and propylene oxide blocks, respectively), was selected as the polymeric template. The titania precursor solution was composed of TiCl₄:EtOH:H₂O:F127 with a molar ratio of 1:40:5:0.005. After deposition, samples were calcined in air at 450 °C for 10 min by a fast-firing process in order to remove the template. Film thickness, volume, and pore size distribution values were obtained from EEP (SOPRA GES5A). Film porosity was obtained by the WinElli 2 software (Sopra Inc.) and pore sizes distributions were derived according to a Kelvin model. SEM images were taken with a Zeiss Leo 982 Gemini electron microscope using the secondary-electron mode and an in-lens detector to improve resolution. TEM images were obtained using a Phillips CM 200 electron microscope.

Thermally Driven Fluid Actuation Experiments: In order to thermoelectrically manipulate the fluids into the mesoporous films, the silicon substrate was brought into contact with a thermoelectric cell (SF-COM-10080, Sparkfun Electronics) connected to an I–V Source Measure Unit (SMU) Keithley 2612A. Temperature values were acquired with a Pt100 Resistance Temperature Detector in contact with the sample. All experiments were carried out by placing drops of water (2 μL) on the mesoporous film. Fluid motion was followed using a Mitutoyo FS70 microscope and movies were recorded by a high resolution digital camera (Pixelink, resolution: 2592 × 1944 pixels) Intensity color profiles were plotted with a software for images analysis (ImageJ), drawing a straight line between both landmarks. The normalized color intensity is given by: $I_n = (I_{max} - I) / (I_{max} - I_{min})$, where I_{max} and I_{min} are the maximum and minimum color intensity, respectively. The reported distances correspond to an average of three measurements.

Supporting Information

Supporting Information is available from the Wiley Online Library or from the author.

Acknowledgements

M.M. acknowledges the doctoral fellowship from Comisión Nacional de Energía Atómica (CNEA), Argentina. The authors thank Andrés Di Donato for his collaboration in the setup of the thermoelectric cell. This work was supported by CONICET (PIP- 0363) and ANPCyT (PICT-2015-1051 and PICT-2016-1781), Argentina.

Conflict of Interest

The authors declare no conflict of interest.

Keywords

fluid manipulation, mesoporous materials, nanofluidics, thin films

Received: August 8, 2017

Revised: September 19, 2017

Published online:

-
- [1] W. Sparreboom, A. van der Berg, J. C. T. Eijkel, *Nat. Nanotechnol.* **2009**, *4*, 713.
- [2] L. Bocquet, P. Tabeling, *Lab Chip* **2014**, *14*, 3143.
- [3] M. G. Bellino, I. Tropper, H. Duran, A. E. Regazzoni, G. J. A. A. Soler-Illia, *Small* **2010**, *6*, 1221.
- [4] T. Brezesinski, J. Wang, J. Polleux, B. Dunn, S. H. Tolbert, *J. Am. Chem. Soc.* **2009**, *131*, 1802.
- [5] R. M. Gazoni, M. G. Bellino, M. C. Fuertes, G. Giménez, G. J. A. A. Soler-Illia, M. L. M. Ricci, *J. Mater. Chem. C* **2017**, *5*, 3445.
- [6] N. Hidalgo, M. E. Calvo, M. G. Bellino, G. J. A. A. Soler-Illia, H. Míguez, *Adv. Funct. Mater.* **2011**, *21*, 2534.
- [7] B. Naik, N. N. Ghosh, *Recent Pat. Nanotechnol.* **2009**, *3*, 213.
- [8] P. Innocenzi, L. Malfatti, *Chem. Soc. Rev.* **2013**, *42*, 4198.
- [9] G. Soler-Illia, P. Angelomé, M. Fuertes, A. Calvo, A. Wolosiuk, A. Zelcer, M. Bellino, E. Martínez, *J. Sol-Gel Sci. Technol.* **2011**, *57*, 299.
- [10] M. Mercuri, K. A. Pierpauli, M. G. Bellino, C. L. Berli, *Langmuir* **2016**, *33*, 152.
- [11] D. R. Ceratti, M. Faustini, C. Sinturel, M. Vayer, V. Dahirel, M. Jardat, D. Grosso, *Nanoscale* **2015**, *7*, 5371.
- [12] J. Lee, T. Laoui, R. Karnik, *Nat. Nanotechnol.* **2014**, *9*, 317.
- [13] P. Huber, *J. Phys.: Condens. Matter* **2015**, *27*, 103102.
- [14] M. Mercuri, K. A. Pierpauli, C. L. Berli, M. G. Bellino, *ACS Appl. Mater. Interfaces* **2017**, *9*, 16679.
- [15] Y. Xue, J. Markmann, H. Duan, J. Weissmüller, P. Huber, *Nat. Commun.* **2014**, *5*, 4237.
- [16] G. Kwon, D. Panchanathan, S. R. Mahmoudi, M. A. Gondal, G. H. McKinley, K. K. Varanasi, *Nat. Commun.* **2017**, *8*, 14968.
- [17] C. J. Brinker, G. W. Scherer, *Sol-Gel Science: The Physics and Chemistry of Sol-Gel Processing*, Academic Press, UK **2013**.
- [18] F. J. DiSalvo, *Science* **1999**, *285*, 703.
- [19] R. Venkatasubramanian, E. Siivola, T. Colpitts, B. O'quinn, *Nature* **2001**, *413*, 597.
- [20] T. Harman, P. Taylor, M. Walsh, B. LaForge, *Science* **2002**, *297*, 2229.
- [21] M. M. Hamed, A. Ainla, F. Güder, D. C. Christodouleas, M. T. Fernández-Abedul, G. M. Whitesides, *Adv. Mater.* **2016**, *28*, 5054.